Bistatic Ground-Based Synthetic Aperture Radar

Bistatic Ground-Based Synthetic Aperture Radar

Massimiliano Pieraccini, DINFO University of Florence, massimiliano.pieraccini@unifi.it, Italy
Lapo Miccinesi, DINFO University of Florence, lapo.miccinesi@unifi.it , Italy

Abstract

GBSAR (Ground-Based Synthetic Aperture Radar) systems are popular remote sensing instruments for detecting the ground changes of landslides, glaciers, open pits, as well as for detecting small displacements of large structure as bridges and dams. Recently (2017) a novel mono/bistatic GBSAR configuration has been proposed to acquire two different components of the displacement of the targets in the field of view. In this paper the bistatic theory of GBSAR is developed, formulas for range and angular resolutions are derived. Finally theoretical findings are experimentally verified

1 Introduction

Ground-Based Synthetic Aperture Radar (GBSAR) systems are popular remote sensing instruments for detecting the ground changes of landslides [1], glaciers [2], snow avalanches [3], open pits [4] as well as for detecting small displacements of large structures as bridges [5] and dams [6]. These radars are able to provide displacement maps of the structure under test, but have a critical limitation: they only detect the displacement component along the range direction. By using two GBSAR systems Severin et al. [4] demonstrated the advantage of the vector displacement in slope monitoring. Dei et al. [7] experimentally showed how the detection of only one component could give paradoxical results in structural monitoring (a bridge deck that apparently is raised when loaded). Recently the authors of this paper proposed in a Letter [8] a novel mono/bistatic GBSAR configuration for retrieving the displacement vector. As in that Letter only the bistatic working principle is reported without a theoretical discussion, in this paper the bistatic theory of GBSAR is developed, formulas for range and angular resolutions are derived and even verified experimentally.

2 The Bistatic GBSAR Working Principle

The working principle of the Bistatic GBSAR is shown in Figure 1. A linear monostatic GB-SAR using a third antenna (or rotating one of the other antennas) can acquire an image exploiting the bouncing of the signal through a transponder. The transponder consists of a couple of antennas and an amplifier.

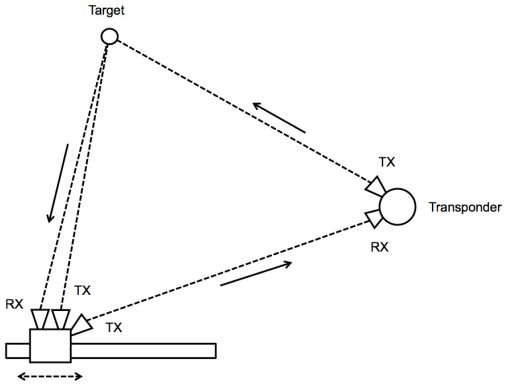

Figure 1: Working principle of Bistatic GBSAR.

Generally speaking, the result of a measurement is a matrix $N_f \times N_p$ of complex numbers:

$$E_{i,k} = I_{i,k} + jQ_{i,k} \tag{1}$$

where $I_{i,k}$ and $Q_{i,k}$ are the in-phase and the quadrature components acquired at i-th frequency ($1<i<N_f$) in the k-th position along the rail ($1<k<N_p$). Focusing in a generic point identified by the polar coordinate (r,φ) means to compensate the phase history of any path radar-point-transponder-radar. With reference to Figure 2, the basic formula is

$$I(r,\phi) = \frac{1}{N_f N_p} \sum_{i,k} E_{i,k} e^{j\frac{2\pi}{c} f_i \left(R(r,\phi,k)\right)} \tag{2}$$

$$R(r,\phi,k) = d_1(k) + d_2(r,\phi) + d_3(r,\phi,k) \tag{3}$$

where $d_1(k)$ is the distance between the transponder and the k-th position of the radar along the rail, $d_2(r,\varphi,k)$ is the distance between the image-point and the k-th position of the antenna on the circle.

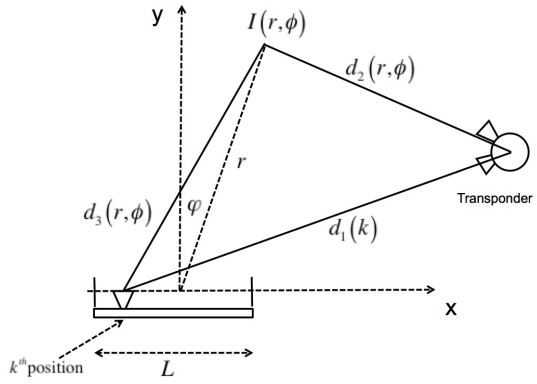

Figure 2: Geometry of the focusing algorithm

The direct application of (2) gives images with high side lobes (-13dB below the main lobe), and this can be a problem. For this reason windowing along both columns and raws has to be applied to the matrix $E_{i,k}$ before to focus it. For example by using a Kaiser window with $\beta_0 = 5$ the side-lobes result lower then -35dB.

3 Range and Angular Resolution

Generally speaking, the radar image of single point target in the coordinate (r_0, φ_0) is not a delta-Dirac but is a function of r, φ, and θ. This function is named Point Spread Function (PSF). As an example we have numerically calculated the PSF of a point target in the position $x_0 = 5$ m, $y_0 = 20$ m. The transponder is positioned in $x_T = 10$ m, $y_T = 2$m. The parameters we used are: $f_c = 10$ GHz, $B = 160$ MHz, $L = 2$ m, $N_f = 401$, $N_p = 301$. Figure 3 shows the PSF in Cartesian coordinates in log scale.

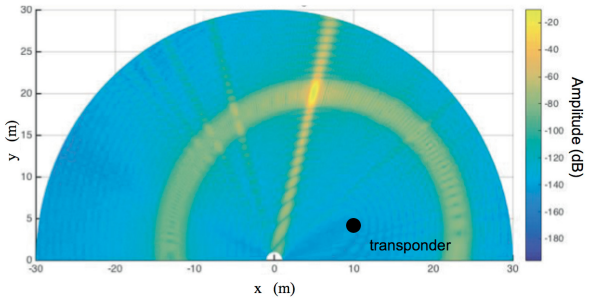

Figure 3: PSF in Cartesian coordinates of a point in (5 m, 20 m)

For estimating the range resolution we can refer to Figure 4. We consider the path C-A-T and the path C-B-T. They are separated in time if their difference is larger then the time resolution c/B, with c speed of light and B bandwidth.

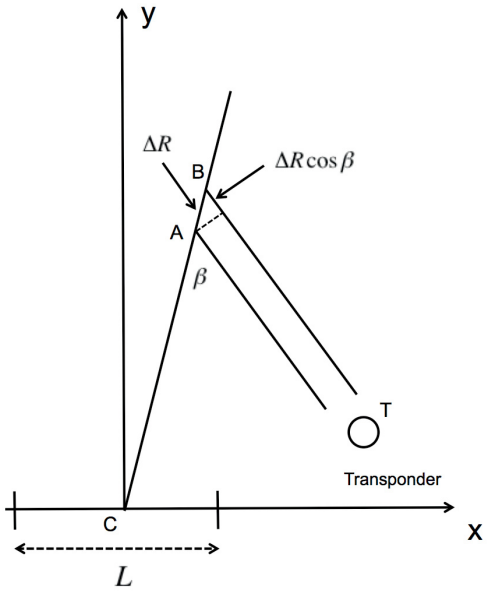

Figure 4: Estimation of range resolution

Therefore we write

$$\Delta R + \Delta R\cos\beta = \frac{c}{B} \tag{4}$$

that is

$$\Delta R = \frac{c}{2B}\Big/\cos^2\left(\frac{\beta}{2}\right) \tag{5}$$

that is the expression we searched. It is worth to note as it differs from the well-known range resolution for a monostatic radar only for its dependence on the angle β and it coincides with the later when $\beta = 0$. The resolution given by eq. (5) is in effect the half-distance (w) between the first two zeros of a sinc. It is often more practical to use the Full Width at Half Maximum (FWHM), that is equal to $1.21w$. By windowing the $E_{i,k}$ in frequency domain the resolution worsens of factor $\delta > 1$ that depends on specific window, as an example for a Kaiser window with $\beta_0 = 5$, $\delta = 1.501$. Finally we can write:

$$FWHW_R = 1.207\,\delta\frac{c}{2B}\Big/\cos^2\left(\frac{\beta}{2}\right) \tag{6}$$

For estimating the angular resolution we have to take into account that the locus of points at the same time-delay are the points of the ellipse that has the scan center (0,0) and the transponder (x_T, y_T) as foci (see Figure 5). Therefore it is convenient to define the angular resolution $\Delta\varphi_C$ with respect to the point (x_C, y_C) along the bisector of angle β crossing the straight line joining the scan center (0,0) and the transponder (x_T, y_T). If we shift

ISBN 978-3-8007-4636-1 / ISSN 2197-4403

the origin of axes in the point (x_C,y_C) the angular resolution will result well-defined.

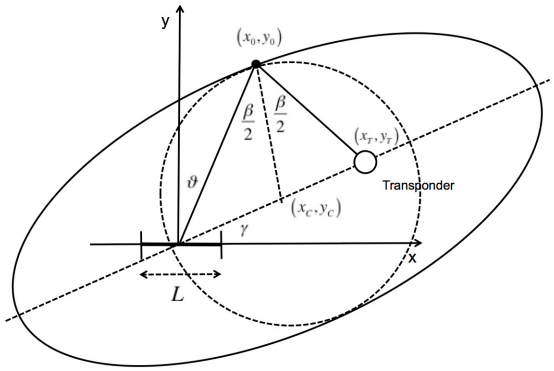

Figure 5: Constant time-delay ellipse

By elementary geometrical considerations:

$$x_C = R_C \cos(\gamma) \quad y_C = R_C \sin(\gamma) \tag{7}$$

where R_C is the distance of (x_C,y_C) from the origin of axes. It can be obtained as

$$R_C = \left|\sin\left(\frac{\beta}{2}\right) \Big/ \cos\left(\vartheta + \gamma - \frac{\beta}{2}\right)\right| R_0 \tag{8}$$

For estimating the quantitative value of the angular resolution $\Delta\varphi_C$ we can refer to Figure 6. The angular resolution $\Delta\theta$ can be calculated as resolution given by a physical aperture L at an angle θ, therefore

$$\Delta\vartheta = 1.207 \frac{\lambda}{L\cos\vartheta} \tag{9}$$

It results with elementary geometrical considerations

$$\Delta\vartheta R_0 / \cos(\beta/2) = \Delta\phi_C R_A \tag{10}$$

Therefore

$$\Delta\phi_C = 1.207 \frac{R_0}{R_A \cos(\beta/2)} \frac{\lambda}{L\cos\vartheta} \tag{11}$$

Figure 6: Geometry for the calculus of the angular resolution

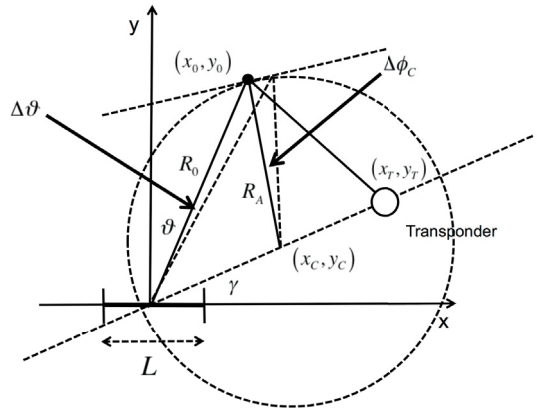

4 Radar and transponder

The Figure 7 shows a sketch of the radar prototype we assembled.

Figure 7: The radar prototype

A vector network analyzer (VNA) HP8720D operated

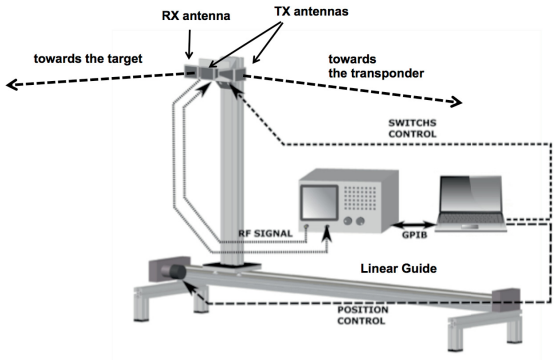

as transceiver providing a continuous wave stepped frequency signal (CWSF) in X-band with central frequency f_c =10 GHz and bandwidth B =160 MHz. Two RF cables linked the VNA to the front-end that scan along a mechanical axis. The Figure 8 shows a sketch of the transponder.

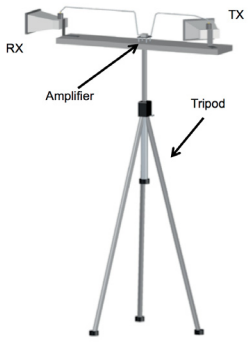

Figure 8: The transponder

It consisted of two horns and two wideband amplifiers (Nominal gain: 24 dB, Band: 6-18 GHz, Noise Figure: 5 dB) on a tripod.

5 Experimental test

For testing the capability to obtain bistatic radar images we installed the GBSAR and the transponder in a garden of the University. At about 35 m in front of the radar there was a metallic fence, on the right a line of trees and a metallic signpost. The parameters we used has been L = 1.80 m, N_p = 240, f_c = 10 GHz, B = 160 MHz, N_f = 801. The transponder has been installed on the x-axis at 10 m on the left of the radar.

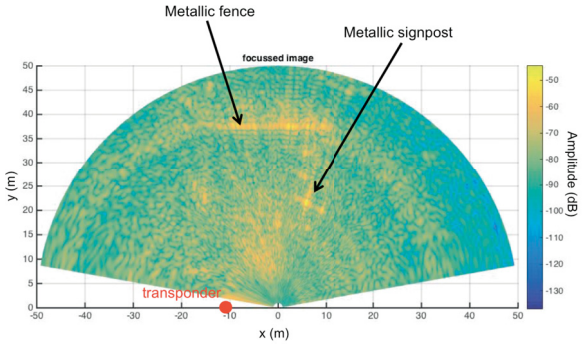

Figure 9: Bistatic radar image

Figure 10 shows the plot of the amplitude in function of φ_C (the angle with respect to (x_C,y_C)) at the range of the metallic signpost that gives the maximum signal in the bistatic image. The plot relative to the target has been compared with the simulation of a point-target. The two plots have been normalized at their maximum. The agreement is excellent and it confirms the theory and the simulation of the previous sections of this paper.

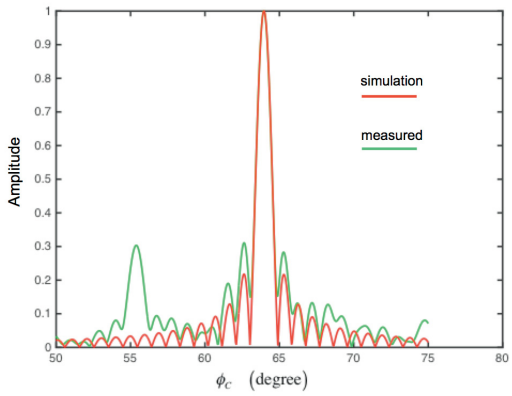

Figure 10: Measured angular plot of the metallic signpost compared with the simulation of a point-target

6 Mono/bistatic operation

As described in [8], both components of the displacement can be obtained with two measurements. In the first measurement the radar operates in monostatic modality and the transponder is switched off. In the second measurement a SPDT (Single Pole Double Through) switches the power to a second antenna that is pointed at the transponder (that is switched on). In this way a bistatic acquisition is performed. The monostatic modality allows obtaining the component along the direction of view of the radar, while the bistatic modality gives the component along the bisector of the angle between radar and transponder.

A possible critical issue of the bistatic modality is the long-term phase stability of the transponder that could affect the displacement measurement. However, both a possible phase change of the transponder amplifier and a small uncontrolled movement of the mechanical support of the transponder can be treated as a change in the atmospheric phase screen and so can be compensated [9]

7 Conclusions

In this Paper has been theoretically and experimentally demonstrated that, using a transponder, a monostatic linear GBSAR can operate as a bistatic system.

References

[1] L. Noferini, T. Takayama, M. Pieraccini, D. Mecatti, G. Macaluso, G. Luzi, C. Atzeni, "Analysis of ground-based SAR data with diverse temporal baselines." *IEEE Transactions on Geoscience and Remote Sensing*, Vol. 46, No. 6, pp. 1614-1623, June 2008

[2] G. Luzi, M. Pieraccini, D. Mecatti, L. Noferini, G. Macaluso, A. Tamburini, C. Atzeni, "Monitoring of an alpine glacier by means of ground-based SAR interferometry", *IEEE Geoscience and Remote Sensing Letters*, Vol. 4, No. 3, pp. 495-499, July 2007

[3] A. Martinez-Vazquez, J. Fortuny-Guasch, "A GB-SAR processor for snow avalanche identification." *IEEE Transactions on Geoscience and Remote Sensing*, 46(11), 3948-3956, November 2008

[4] J. Severin, E. Eberhardt, L. Leoni, S. Fortin, "Development and application of a pseudo-3D pit slope displacement map derived from

ground-based radar." Engineering Geology, Vol. 181, pp. 202-211, 2014

[5] M. Pieraccini, D. Tarchi, H. Rudolf, D. Leva, G. Luzi, G. Bartoli, C. Atzeni, "Structural static testing by interferometric synthetic radar". NDT & E International, Vol. 33, No. 8, pp. 565-570, 2000.

[6] W. Jenkins, B. Rosenblad, F. Gomez, J. Legarsky, and E. Loehr, "Deformation measurements of earth dams using a ground based interferometric radar," in: Proceedings of the 2012 ASDSO Annual Conference on Dam Safety

[7] D. Dei, D. Mecatti, and M. Pieraccini, "Static Testing of a Bridge Using an Interferometric Radar: The Case Study of ''Ponte degli Alpini,'' Belluno, Italy", The Scientific World Journal, Vol. 2013, Article ID 504958, (2013)

[8] M. Pieraccini, L. Miccinesi, N. Rojhani, N. "A GBSAR Operating in Monostatic and Bistatic Modalities for Retrieving the Displacement Vector." *IEEE Geoscience and Remote Sensing Letters*, Vol. 14, No. 9, pp. 1494-1498, July 2017

[9] R. Iglesias, X. Fabregas, A. Aguasca, J. J. Mallorqui, C. López-Martínez, J. A. Gili, J. Corominas, "Atmospheric phase screen compensation in ground-based SAR with a multiple-regression model over mountainous regions", IEEE Transactions on Geoscience and Remote Sensing, vol. 52, no. 5, pp. 2436-2449, May 2014.